Journal of Food and Agriculture Research
Vol. 5, No. 2, 2025, pp. 163-190
© ARF India. All Right Reserved
URL: www.arfjournals.com
https://doi.org/10.47509/JFAR.2025.v05i02.06

Microstructural Diversity on the Leaf Surface of Peanut Cultivars: Probable Role in Defense

Thejaswini Alavalapati, Birat Sapkota, Poonam Khatri, Aftab Siddique, Thomas H Terrill and Nirmal Joshee*
Agricultural Research Station, Fort Valley State University, Fort Valley, Georgia 31030
**Corresponding author E-mail: josheen@fvsu.edu*

Abstract: This microscopic study focuses on the micromorphological characteristics in four Georgia grown peanut cultivars (Georgia -06, Georgia-12Y, Georgia -20VHO, and Jumbo) with the goal to identify morphological variations associated with the possible fungal tolerance. In this study instead of depending exclusively on overall accuracy or visual overlays, we present class-specific precision, recall, and F1-score metrics, which elucidate significant disparities in the models' management of morphological variability. Variations in the distribution of trichomes, vein endings (VE) and areoles (also known as vein islets), stomatal index and density were observed in leaves. Stomatal studies revealed paracytic stomata in all four cultivars; Georgia-12Y cultivar exhibited anisocytic and paracytic stomata both. Cultivar G-06 scored highest number of VE (173.25±5.99) and areoles (180.55±8.85) on the adaxial leaf surface. The trichomes on the adaxial and abaxial leaf surfaces of G-20 was highest (128.2±6.14; 180±12.27) and significant differences were recorded. Wax crystalloids on the adaxial and wax sheath on the abaxial leaf surface were observed in all cultivars. The highest stomatal density and stomatal index were observed on the abaxial leaf surface of G-12Y (20.40±1.12) and Jumbo (17.47±0.45), respectively. The higher number of calcium and silicon in the inclusions were observed on the leaf margin of Jumbo 12.28±3.33 % and 13.61±2.28 %, respectively. The current leaf micromorphological study of peanut cultivars provides valuable insights in plant surface topography differences and its possible role in the fungal tolerance mechanisms.

***Keywords*:** Aflatoxin, areoles, CNN modeling, cuticle, stomata, trichomes, vein endings.

Received : 22 July 2025
Revised : 26 August 2025
Accepted : 30 August 2025
Published : 03 September 2025

TO CITE THIS ARTICLE:

Thejaswini Alavalapati, Birat Sapkota, & et al. 2024. Microstructural Diversity on the Leaf Surface of Peanut Cultivars: Probable Role in Defense. *Journal of Food and Agriculture Research,* 5: 2, pp. 163-190. *https://doi.org/10.47509/JFAR.2025.v05i02.06*

1. Introduction

Peanut (*Arachis hypogaea* L.; Fabaceae) is recognized as one of the important oilseeds crops globally (Rao and Murty, 1994) which is cultivated in over 80 countries. A total of 12% of global peanut production comes from the USA (FAS-USDA, 2023). Peanuts are a good source of nutrition containing essential fatty acids, proteins, carbohydrates, minerals (calcium, iron, phosphorus, sodium, potassium, and zinc), and bioactive compounds (folic acid, thiamine, and tocopherols) (Isanga and Zhang, 2007; Ayoola *et al.*, 2012; Davis *et al.*, 2016; Liu *et al.*, 2022). Peanuts are susceptible to *Aspergillus* species during pod development and poor post-harvest conditions, producing aflatoxins. This seriously risks human health and agriculture (Akram *et al.*, 2018). In addition to that, there are instances of leaf infection by same *Aspergillus* spp. Yellow mold of peanut caused by *A. flavus* leads to pre-emergence rotting of peanut seed and seedlings resulting in chlorotic plants with reduced size of leaflets exhibiting vein-clearing (Subrahmanyam *et al.*, 1987). Seedling hypocotyls are highly susceptible to *A. niger* causing crown rot disease. Leaf spot diseases of peanut are caused by two distinct, but closely related, fungal plant pathogens (*Cercosporidium personatum*).

Various types of microstructures (cuticle, stomata, trichomes etc.) have been reported on the aerial parts of plants, predominantly on the leaf surface. Plants are endowed with unique foliar microstructures that enable them to retain particulate matter, dust, pollen and pathogen spores, which have a profound impact on the microbial communities. These microscopic structures have been described as an active part of the defense mechanism of plant against biotic and abiotic agents (Dehgahi *et al.*, 2015; Patel *et al.*, 2021). Microscopic features such as vein ending, areoles (AR), trichomes, stomata, and cuticle in the plant leaves participate in protection from various infections and environmental extremes. The VE in leaves facilitate nutrient transfer and contribute to leaf morphology (Esau, 1977). Trichomes provide physical and chemical defense against herbivores, ultraviolet (UV) radiation, water loss, and pathogens. However, the pathogens might penetrate the host plant through the open bases or broken trichomes (Bickford, 2016; Kim 2019). Stomatal pores aid in the water evaporation and the gaseous exchange, and act as a point of entry for pathogens (Driesen *et al.*, 2020). By adjusting stomatal opening, plants have evolved a defense mechanism against pathogens and various environmental factors (stomatal defense mechanism or stomatal immunity) (Meddya *et al.*,2023). However, certain pathogens have developed strategies to penetrate the stomatal defense mechanism as seen in genera *Malus*, *Pyrus*,

Cydonia, and *Mespilus* (Voronkov *et al.*, 2020). Cuticle is the outermost layer of the leaf composed of cutin polyester and waxes, that acts as a physical barrier against water loss and pathogens (Arya *et al.*, 2021). Structure, thickness, and composition of cuticle have been associated with the resistance/tolerance of plants against biotic and abiotic stresses (Gabler *et al.*, 2003; Gomes *et al.*, 2012). Epicuticular wax deposits on the seed coats of peanuts have been inversely related to fungal infection and aflatoxin production, showing that a healthy cuticle may play a protective role in crop health (Goh, 2001; Liang *et al.*, 2003). Hence, leaf epidermal structures such as trichomes, stomata, and cuticle play an important role in mediating plant defense and could be essential traits that impart tolerance to biotic and abiotic stresses (Patel *et al.*, 2021).

In the current study, microstructures such as leaf venation, trichomes (types and morphology), stomata, and cuticle have been studied using microscopic techniques including light and scanning electron microscopy (SEM). The comparative study of micromorphological characteristics among peanut cultivars, which are important during biotic and abiotic stresses, can be used to develop strategies for improving crop yield and tolerance to aflatoxin contamination, resulting in sustainable cultivation practices as has been suggested for many other plants (Wang *et al.*, 2021). While conventional microscopy is useful in studying leaf venation, trichomes, stomata, and cuticles, it often faces limitations due to manual processing and subjective interpretation. These complex microstructures, which serve as essential physiological and protective characteristics, exhibit unique visual patterns that can be harnessed through advanced computer system approaches for breeding programs. To minimize mistakes in the identification and quantification of structures, we used a Convolutional Neural Network (CNN) model to accurately identify the stomata present in leaves using artificial neural networks (Andayani *et al.*, 2020). Convolutional Neural Networks are a robust subset of deep learning models designed to analyze grid-like input, such as images, rendering them particularly adept at computer vision applications. In contrast to conventional fully connected neural networks that consider input properties in isolation, CNNs leverage the spatial organization of data by maintaining the positional correlations among pixels. This design enables the collection of local patterns and the acquisition of hierarchical feature representations, essential for tasks such as image classification, object identification, and segmentation (LeCun *et al.*, 1998; Goodfellow *et al.*, 2016; Raghu *et al.*, 2021). The architecture of a CNN generally comprises convolutional layers, activation functions, pooling layers, and fully connected

layers, each fulfilling a specific and complementary purpose in converting input data into predictions.

The emergence of high-resolution imaging and the increasing availability of annotated datasets have paved the way for CNNs to become effective tools for automating the identification and categorization of microstructures. By utilizing CNNs, one can analyze extensive quantities of micrographs with precision, enabling objective, consistent, and high-throughput examination of microstructures (image-based phenotyping). Here we utilize computer-based approach to quantify microstructure developing two models, taking the example of stomata. The current study aims at filling the knowledge gap by bringing together two technologies (microscopy and computer-based modeling and quantification) for the better understanding of the role of microstructures in plant defense. The transition from manual to AI-assisted phenotyping, with its objectivity, holds significant potential for comparative analyses of peanut cultivars, particularly in the areas of stress tolerance, disease and pest resistance, and breeding.

2. Materials and Methods

2.1. Sample Collection

Seeds of Georgia-06G (G-06), Georgia-12Y (G-12Y), and Georgia-20 VHO (G-20) were obtained from Birdsong Peanuts, Blakely, GA, USA while Jumbo cultivar seeds were bought from Walmart, Warner Robins, GA, USA. Seeds were sown in the Fort Valley State University (FVSU) greenhouse in pots [Pot mixture: cow dung: perlite: vermiculite (3:1:1:1)] and leaves were collected at the time of flowering (July 2023), fixed as specified below, and stored in 70% ethanol at 4◎ until further use.

2.2. Clearing and Micromorphological Analysis

Four fully expanded leaves were collected from one plant for each cultivar and cleared using the method by Vasco *et al.*, 2014 with minor modifications such as changes in ethanol concentration from 50% to 70%, and incubation temperature from 50 ºC to 80 ºC. For the comparative studies of microstructures among the peanut cultivars, leaves were fixed overnight (15 hours approx.) in 70% ethanol at 4 ºC. The fixative ethanol used overnight was discarded and the samples were suspended in fresh 70% ethanol. Leaves in fresh ethanol were incubated at 80°C in a water bath for 30 minutes. This step was repeated four times to ensure removal of pigments and ethanol was changed in each step.

Leaf samples were then suspended in 5% sodium hydroxide (NaOH) solution, incubated at 80°C for five minutes in a water bath, and then allowed to cool at room temperature for 15 minutes. The NaOH solution was decanted, and samples were treated with a 15% (1.13% NaOCl) commercial bleach Clorox (Oakland, CA, USA) solution for 15 minutes at room temperature. Samples were then gently washed with demineralized water until no chlorine smell remained. Cleared leaf samples were then stained with one drop of 0.1% aqueous safranin for one hour. Stained samples were gently rinsed in water to remove safranin. Stained leaves were cut into small pieces as per the required region such as margin, lamina, and midrib and placed on a slide (7.5 cm * 2.5 cm) with a drop of glycerin: demineralized water (1:1), secured with a cover slip and observed under a light microscope (Echo Revolve D115, RVL-100-G).

Microscopic images of cleared mature leaves were taken for adaxial and abaxial leaf surfaces both, for four cultivars (G-06, G12Y, G-20, and Jumbo). The data were collected by scoring the areoles, VE, trichome density (TD), stomatal density (SD), and stomatal index (SI) were calculated as described below:

Trichome Density (TD) = Total Number of Trichomes / Area (1mm^2)

The stomatal index was calculated as suggested by Salisbury, 1928:

Stomatal Index (SI) (%) = (Number of stomata per unit area / Number of stomata + Number of epidermal cells per unit area) ⊚ 100

Stomatal density was calculated using the formula suggested by Paul *et al.*, 2017.

Stomatal density (SD) = Number of stomata/Area (mm^2)

Area = πr^2

$r^2 = (FOV)^2$

FOV = Field Number (FN)/ Objective Magnification (OM)

2.3. *Scanning Electron Microscopy (SEM) and Energy Dispersive X-Ray Spectroscopy (EDX/EDS)*

Plant samples were dried for 48 h in an oven at 37 ⊚, mounted on aluminum stubs using double-sided carbon tape (Electron Microscopy Sciences, PA) and observed using desktop Phenom XL (Nano Instruments, Phoenix, AZ) SEM. Images were captured using SEM with running beam at 15 kV and the same sample was processed with EDS to determine the elemental composition. For studying cuticle, the samples were dried at 37°C, mounted on stubs using

double-sided carbon tape, gold coated, and observed with Hitachi 3400NII VP SEM (Hitachi High-Tech America, Inc., Schaumburg, IL) (Vaidya *et al.*, 2016). Images for cuticle study were captured with running beam at 20kV.

2.4. Developing CNN Model for the Quantitative Analysis of Stomata

2.4.1. Sample Collection

Fifteen fully expanded, mature leaves were collected, cleared, and then observed using the microscope to capture images. One hundred images (jpg format) for each surface were captured (adaxial and abaxial) and subjected to image analysis using CNN model. The same process was followed for all four cultivars to develop CNN models. The following is a description of the process used for developing CNN models (Chen *et al.*, 2019; Jiang *et al.*, 2020; Siddique *et al.*, 2024).

2.4.2. Model 1: A Customized CNN with Batch Normalization and Dropout

Model 1 is a specialized convolutional neural network that incorporates batch normalization and dropout techniques to improve the model's ability to generalize and avoid overfitting. The architecture commences with a convolutional layer with 32 filters of dimensions 3 x 3. This layer employs the Rectified Linear Unit (ReLU) activation function and 'same' padding. Subsequently, batch normalization is used, followed by a max pooling layer to decrease the spatial dimensions. Implementing a dropout rate of 20% is used as a strategy to mitigate overfitting. This pattern recurs with progressively larger filter sizes (64 and then 128 filters) and escalating dropout rates (30% and 40% respectively) at each step. Following the convolutional layers, the model transforms the output into a flat representation and feeds it into a dense layer consisting of 128 neurons. The next step involves applying a softmax activation layer, which is specifically designed to classify the four different stomata classes. The model employs the Adam optimizer and utilizes sparse categorical cross entropy as its loss function, with accuracy serving as the performance parameter.

2.4.3. Model 2: Basic CNN with RMSprop Optimization Algorithm

Model 2 streamlines the method by excluding batch normalization and prioritizing a direct convolutional structure with the RMSprop optimizer, highlighting its ability to adaptively adjust the learning rate. The model has three

convolutional layers with ascending intricacy (32, 64, and 128 filters, all with a 3 x 3 kernel size and 'identical' padding), each subsequently accompanied by a max pooling layer to gradually diminish the feature dimensions. The network incorporates a dense layer consisting of 128 neurons, along with a softmax layer for class prediction once the pooling characteristics have been flattened. The model particularly utilizes the RMSprop optimizer, with an initial learning rate of 0.001, and employs sparse categorical cross entropy for loss computation.

2.4.4. Model Development

This study involved the development of image recognition models using CNNs. The models were developed using a dataset of 100 images obtained with an Echo Revolve D115 microscope. This dataset was carefully selected and organized to meet the exact requirements of deep learning in image classification, with a focus on the significance of high-resolution and clearly defined images for optimal model training. The study utilized the functionalities of Google Colab, a powerful, cloud-based Python programming environment that easily interfaces with Google Drive. This integration simplifies data management enabling the exploitation of Google Colab's Graphic Processing Units (GPU) resources. Having GPUs is crucial in deep learning as they expedite computing operations, leading to a substantial decrease in the time needed for training and processing intricate neural network models. Data management was effectively managed using Google Drive, where all images were kept and categorized into three separate directories, especially designated for training, validation, and testing purposes. This organizational method ensured that the transfer of data into the machine learning pipeline was efficient and well-organized. The tf.keras.utils.image_dataset_from_directory method in TensorFlow was used to automatically process each image dataset and assign labels to the images based on their directory structure. In addition, our technique rescaled photos to a consistent size of 512 x 512 pixels and organized them into sets of 20. Batching improves the efficiency of the training process by ensuring that the model can handle substantial amounts of data without sacrificing performance. Two CNN architectures were created and executed for image classification. The initial model was a CNN specifically designed and constructed, incorporating layers for batch normalization 18 and dropout. Batch normalization is a technique that helps to stabilize the learning process, ensuring that the average output is kept near to zero and the standard deviation of the output is kept close to one. Dropout layers were included to mitigate overfitting, a prevalent issue in neural network training when the model acquires knowledge of the irrelevant

details in the training data to such an extent that it adversely affects the model's ability to perform well on fresh data.

The second model utilized the RMSprop optimizer, which is well-known for its effectiveness in dealing with noise issues and its ability to adaptively alter the learning rate for each parameter. This model was specifically designed to improve training convergence, enabling faster attainment of lower loss and improved accuracy during the training phase by efficiently updating the network weights. In summary, the study's dedication to utilizing state-of-the-art technologies, such as advanced CNN models and efficient data management in a robust computational platform like Google Colab, highlights its focus on achieving accurate and dependable outcomes in the realm of image classification. This strategy guarantees strong and reliable model performance and establishes a standard for future study using deep learning techniques for intricate image data.

2.4.5. Data Analysis

Data was analyzed through Analysis of variance (ANOVA) procedures of the Statistical Analysis System (version 9.4, SAS Institute Inc., Cary, NC), followed by Tukey's Post-hoc mean separation test with the least significant difference at $P \leq 0.05$ for areoles, VE, trichomes, stomatal index, and stomatal density (n= 20 for areoles, VE, and trichomes; n= 9 for stomatal density and stomatal index).

3. Results and Discussion

3.1. Characterizing Micromorphological Structures

3.1.1. Vein Endings and Areoles

The VE on adaxial leaf surfaces of peanut cultivars (G-06, G-12Y, and G-20) were hooked, straight, and branched, while in the Jumbo cultivar they were mostly unbranched and hooked and straight (Fig. 1). The quantitative analysis of all the cultivars showed a high number of VE on the adaxial leaf surface (G-06 - 173.25±5.99; G-12Y - 58.1±2.93; G-20 - 144.8±9.56; Jumbo - 137.1±7.02) compared to the abaxial leaf surface (G-06 - 168.4±6.08; G-12Y - 58.4±1.77; G-20 - 123.55±6.93; Jumbo - 133.15±6.41) in a unit area (Table 1). The adaxial leaf surface showed high number of areoles (G-06 -180.55±8.85; G-12Y - 52.25±3.22; G-20 - 176.25±12.55; Jumbo - 147.25±5.26) compared to the abaxial leaf surface (G - 06 - 175.75±5.00; G-12Y - 55.55±1.42; G-20 - 157.4±7.08; Jumbo - 162.35±9.36) except the G-12Y where abaxial leaf surface have higher number of areoles

compared to the adaxial leaf surface. The G-06 cultivar showed the highest number of VE and areoles, combining both surfaces, among all the cultivars studied (Table 1). The ANOVA showed statistically significant differences at

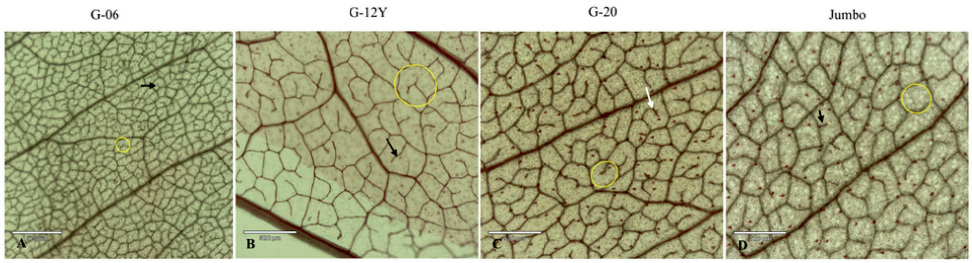

Figure 1: Microscopic images of cleared leaf samples in peanut cultivars to show vein termination types and different sizes of areoles. A. G-06 peanut cultivar, B. G-12Y peanut cultivar, C. G-20 peanut cultivar, D. Jumbo peanut cultivar. Yellow circles indicate areoles in each cultivar. Black arrows indicate straight vein termination whereas white arrow shows hooked vein termination points. (Scale 520 μM).

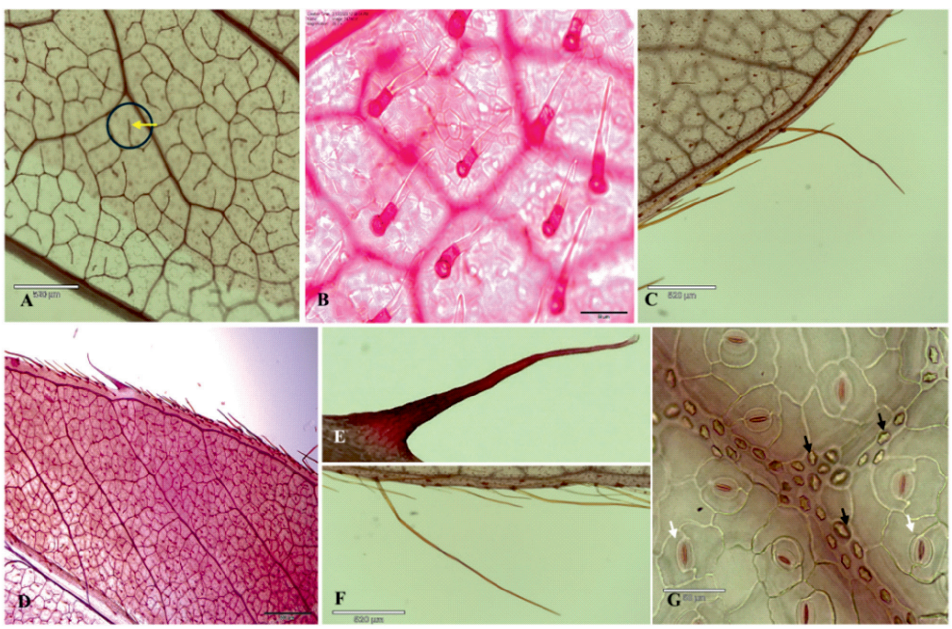

Figure 2: Microstructures observed on the cleared leaf samples of peanut cultivars. A. Vein ending (arrow indicating vein ending) and areoles (circle showing areoles) of G-12Y adaxial leaf surface. B. Trichomes on the surface of Jumbo cultivar, basal cells taking darker stain. C. Non-glandular trichomes of variable lengths on the leaf margin of G-20 cultivar. D. Diverse trichomes on Jumbo abaxial leaf margin. E, F. Two types of non-glandular trichomes observed on the margin of Jumbo cultivar. G. Inclusions (black arrows) and stomata (white arrows) on the adaxial leaf surface of Jumbo cultivar. (Scale: A, C, F: 520 μM; B, G: 50 μM; D. 500 μM; E. 210 μM).

P≤0.05 among the cultivars for the VE and areoles. Variance in VE were observed in Acer leaves, as a function of specific location of analysis contributing to the observed differences (Banerji and Das, 1972). This study provides further information on the minor venation of 150 species from Euphorbiaceae family (Sehgal and Paliwal, 1974) and 15 species from the genus '*Salix*', where the minor venation was found to be unhelpful in identifying the species (Singh *et al.*, 1976). Similar results were found in the genus *Salvia* (Lamiaceae) where out of the nine species, only two could be distinguished based on their venation patterns. The variation observed among the cultivars for these microstructures/ morphological characters (VE and areoles) in our study could add information regarding these cultivars that could be helpful for their taxonomical studies.

Table 1: Presence or absence of microstructures in various leaf parts of peanut cultivars. Vein endings (VE), areoles (AR), and non-glandular trichomes (NT). The data is presented as Mean ± Standard error (S.E.).

Leaf surface	*Cultivars*	*VE*	*AR*	*NT*			*Multicellular NT*
			Lamina	*Midrib*	*Margin*		
Adaxial	G-06	173.25±5.99	180.55±8.85	14.8±1.82	3.05±0.97	8.7±0.46	0
	G-12Y	58.1±2.93	52.25±3.22	46.8±7.60	5.7±1.37	25.4±2.26	0
	G-20	144.8±9.56	176.25±12.55	128.2±6.15	12.05±1.42	30.1±3.01	0
	Jumbo	137.1±7.02	147.25±5.26	124.9±5.58	21.7±3.18	29.2±2.17	0.7±0.19
Abaxial	G-06	168.4±6.08	175.75±5	35.75±1.40	6.95±2.14	10.25±0.54	0
	G-12Y	58.4±1.77	55.55±1.42	53.7±6.13	7.45±1.51	15.9±1.35	0
	G-20	123.55±6.93	157.4±7.08	180.8±12.27	29.95±2.87	39.45±1.94	0
	Jumbo	133.15±6.41	162.35±9.36	195.05±20.74	25±2.55	33.05±1.98	1.2±0.16

3.1.2. Trichomes

Trichomes present on the leaves of the peanut cultivars are smooth-surfaced unicellular non-glandular trichomes, except the Jumbo cultivars (Table 2). It has multicellular non-glandular trichomes on leaf margins without protruding bases (Fig. 2, D-F) and are equally distributed. More number of trichomes were present on the adaxial leaf surface on lamina (G - 12Y - 46.8±7.59; G – 06 - 14.8±1.81; G – 20 - 128.2±6.15; Jumbo - 124.9±5.57) and midrib region (G - 12Y – 5.7±1.37; G – 06 – 3.05±0.97; G – 20 –12.05±1.42; Jumbo – 21.7±3.18). The abaxial leaf surface has more trichomes in the margin region (G–06 – 10.25±0.54; G–12Y – 15.9±1.35; G–20 – 39.45±1.94; Jumbo – 33.05±1.98). Range of variation in leaflet trichome density was observed across peanut cultivars (Fig. 3). Trichome density on the adaxial leaf surface was less as compared to the abaxial leaf surface (Fig. 4). We also observed the presence of trichomes

on the midrib abaxial leaf surface; however, no trichome was observed on the adaxial leaf surface (Fig. 4).

Table 2: Types of trichome and vein ending on the adaxial and abaxial leaf surface of peanut cultivars

Cultivar	*Surface*	*Type of trichome*	*VE Type*	*VE Branches*
G-06	Adaxial	Unicellular non-glandular	Hooked and straight	Branched
	Abaxial	Unicellular non-glandular	Hooked and straight	Branched
G-12Y	Adaxial	Unicellular non-glandular	Hooked and straight	Branched
	Abaxial	Unicellular non-glandular	Straight	Branched
G-20	Adaxial	Unicellular non-glandular	Hooked and straight	Branched
	Abaxial	Unicellular non-glandular	Hooked and straight	Branched
Jumbo	Adaxial	Unicellular non-glandular	Straight	Unbranched
	Abaxial	Unicellular non-glandular and Setose Hirsute non-glandular trichome	Straight	Unbranched

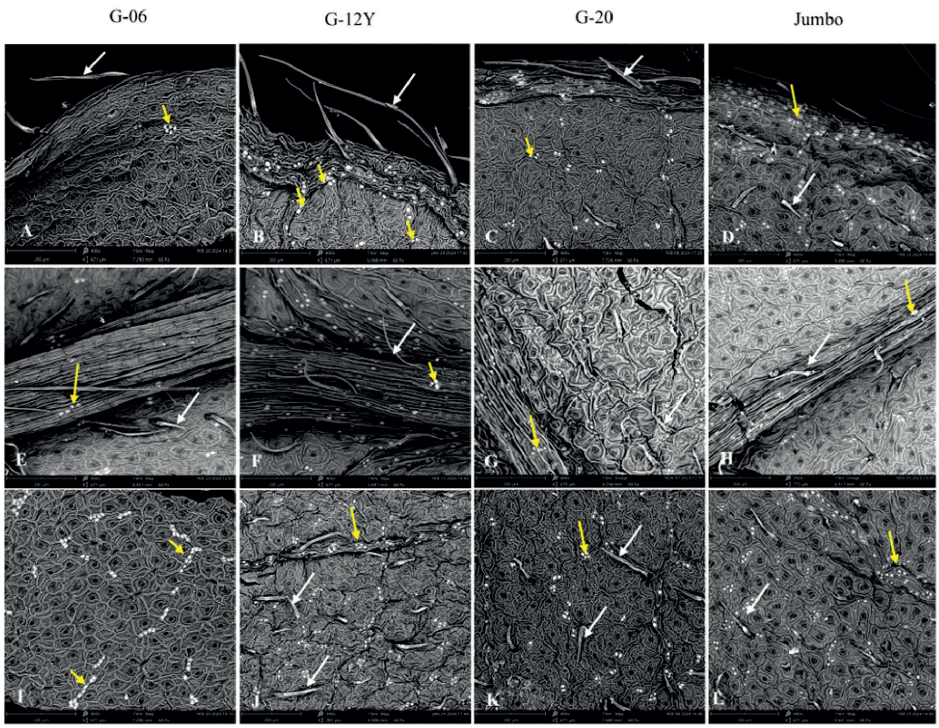

Figure 3: Scanning electron micrograph of inclusion patterns and trichome distribution on the abaxial leaf surface (margin, midrib, lamina) of peanut cultivars. A-D: Inclusion patterns on the margin of G-06, G-12Y, G-20, and Jumbo cultivars. E-H: Inclusion patterns and trichome distribution on abaxial leaf midrib tissues in peanut cultivars. I-L: Inclusion patterns and trichome distribution on the abaxial leaf lamina in peanut cultivars. Yellow arrows indicate inclusions. White arrows indicate trichomes. Magnification: 400X.

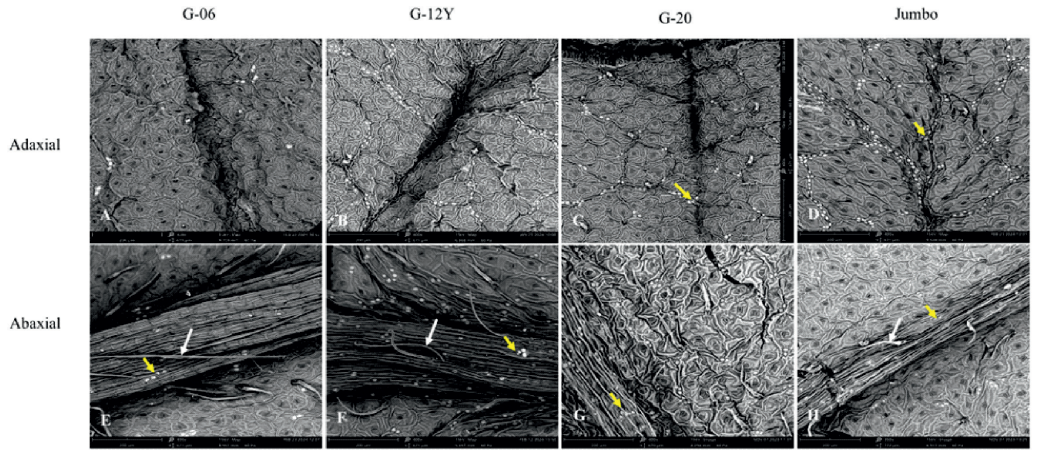

Figure 4: Study of leaf midrib in G-06, G-12Y, G-20 and Jumbo cultivars for the presence of inclusions in peanut cultivars using scanning electron microscope. A-D: Adaxial midrib leaf surface and E-H: Abaxial midrib leaf surface showing distinct inclusion patterns (yellow arrows). E-H: White arrows indicate unicellular non-glandular trichome on the leaf midrib on the abaxial surface, respectively. Magnification: 400X.

Simple non-glandular trichomes often function as a deterrent to insects. Trichomes in wine grape leaves (*V. vinifera* L.) serve as a defensive mechanism against photo-damage during leaf growth. The function of trichomes provides evidence that the presence of both simple and ribbon trichomes on grape leaves serves as a protective barrier, effectively limiting the growth of fungus and preventing fungal hyphae from reaching the leaf cuticle (Karabourniotis *et al.*, 1999; Kortekamp and Zyprian, 1999; Liakopoulos *et al.*, 2006). These structures are recognized for their protective functions, such as mechanical deterrents against herbivores and pathogens. The variation was observed for the presence of trichomes among the cultivars in our study which would help to study their roles in plant defense mechanisms against biotic or abiotic factors.

3.1.3. Stomata

In this study, it was observed that all four cultivars were amphistomatic and the stomata were predominantly paracytic (Fig. 5). Paracytic stomata possess two subsidiary cells positioned parallel to the guard cells, and these subsidiary cells bear a resemblance to the epidermal cells. The quantitative analysis in all the cultivars (Fig. 6) showed a high number of stomatal density on the abaxial leaf surface (G-06 - 2.70±0.96; G-12Y- 3.56±1.26; G-20 -4.043±1.35; Jumbo- 3.14±1.11) compared to the adaxial leaf surface (G-06 – 1.88±0.67; G-12Y - 2.33±0.82; G-20 – 2.87±0.96; Jumbo - 3.14±1.11). The abaxial leaf surface showed high number

of stomatal index G-06 – 2.25±1.14; G-12Y- 3.04±1.70; G-20 – 3.12±1.47; Jumbo-2.55±2.55) compared to the adaxial leaf surface (G-06 - 1.14±0.40; G-12Y - 1.70±0.60; G-20 - 1.47±49; Jumbo - 2.55±0.90). The ANOVA showed statistically significant differences at $P \leq 0.05$ among the cultivars for the stomatal density and stomatal index.

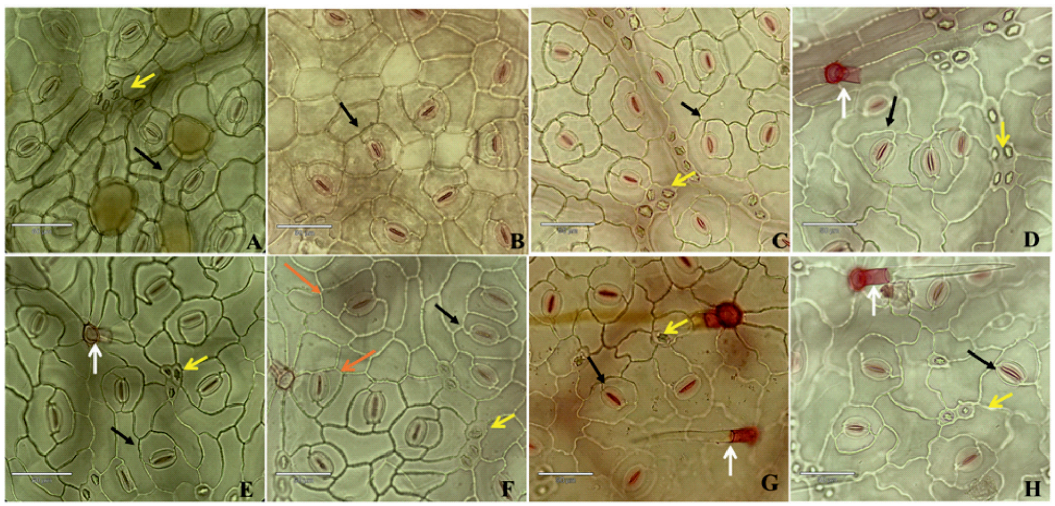

Figure 5. Light microscope images of stomatal structures on peanut leaves. A–D: Adaxial leaf surface showing inclusions (yellow arrows) and paracytic stomata (black arrows) in G-06, G-12Y, G-20, and Jumbo cultivars. E: Abaxial surface of G-06 showing inclusions (yellow arrows), paracytic stomata (black arrows), and a unicellular non-glandular trichome (white arrows). F: G-12Y abaxial surface with anisocytic stomata (orange arrows) and inclusions (yellow arrows). G–H: Abaxial surfaces of G-20 and Jumbo showing paracytic stomata (black arrows) and inclusions (yellow arrows). Magnification: 40X.

The type of stomata, number of subsidiary cells in contact with guard cells were recorded for their size, shape, number, and morphology (Gray *et al.*, 2020). Stomata are leaf surface structures primarily responsible for gas exchange. However, in certain instances, pathogens can also penetrate through these stomata. The stomata are formed by the guard cells with the stomatal pore between them (Sack, 1987). The stomata are accompanied by subsidiary cells, which are style based on the number of subsidiary cells linked to each stoma. The phyllosphere is a crucial environment for microbial colonization. This environment helps the viability and proliferation of microorganisms such as fungi and bacteria. Fungal or bacterial entry can occur by several pathways, including stomata (Melotto *et al.*, 2006). The plant is also incapable of defending against fungal invasion via the stomatal pores. Stomata are tiny pores found

on the epidermis of leaves, stems, and other organs, consisting of two distinct guard cells. Stomata are utilized by plants to facilitate the exchange of gases and other physiological processes and regulate transpiration by regulating the aperture width (Franks and Farquhar, 2007). Plants regulate the opening and closing of these pores by adjusting the turgor pressure in the guard cells. Various environmental stimuli, including factors like light intensity, air humidity, CO_2 concentration, and drought stress, have an impact on stomatal movements (Underwood *et al.*, 2007). Our study on stomatal density and stomatal index showed significant differences among the cultivars. In addition to that, the presence of various types of stomata was observed among the cultivars, which could suggest the variation in the plant defense as there is variation in the number of stomata present as well as their types.

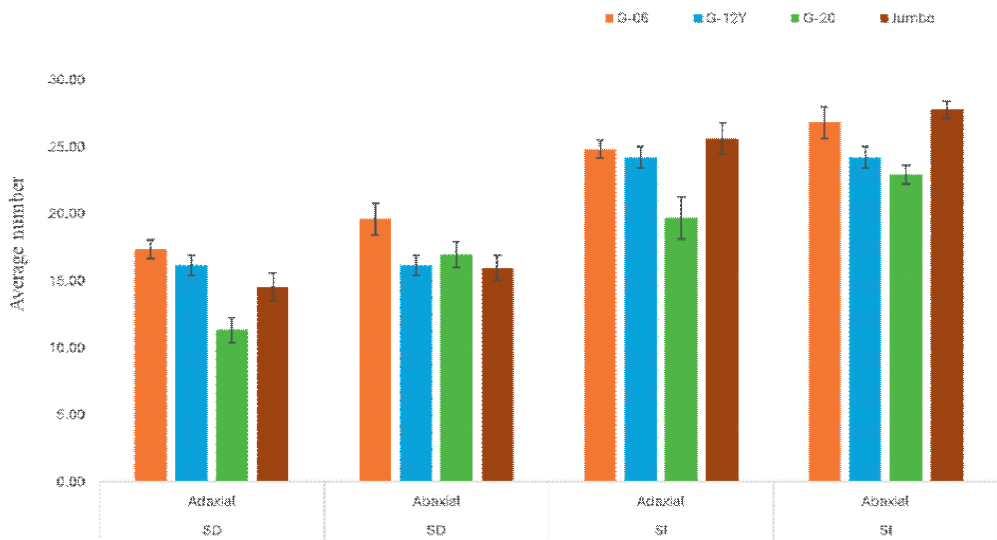

Figure 6: Stomatal Density (SD) and Stomatal Index (SI) in the leaves of G-06, G-12Y, G-20, and Jumbo peanut cultivars. Each value represents Mean ± S.E. Significant differences were observed for SD and SI among the cultivars at $P \leq 0.05$.

3.1.4. Cuticle

In the current study, two types of cuticles were observed on leaf surfaces based on their morphology. It was evident that the adaxial surface was covered with crystalloids/ platelets wax while the abaxial surface was observed as covered by the epicuticular wax sheath in all four peanut cultivars (Fig. 7, A-H), the difference in the wax deposition in the adaxial and abaxial surface in same cultivar was observed (Fig. 7, I-J).

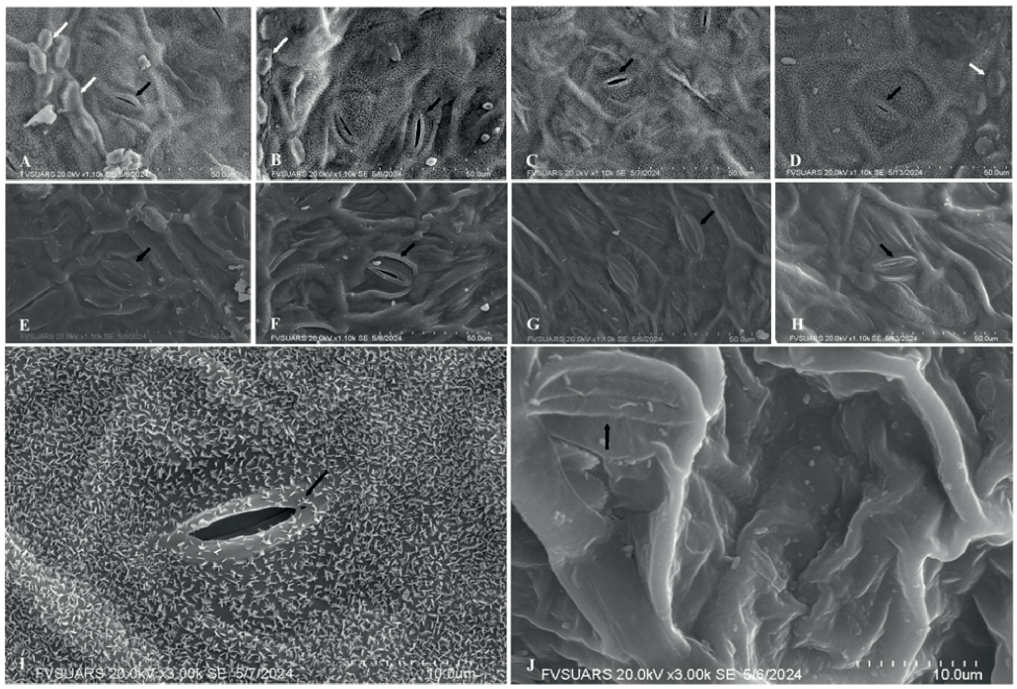

Figure 7: Differential wax deposition pattern on the adaxial and abaxial surfaces in the leaves of peanut cultivar under SEM. Adaxial: Wax crystalloids / platelets in A. G-06, B. G-12Y, C. G-20, and D. Jumbo; Abaxial: Cuticle is seen as epicuticular wax sheath E. G-06, F. G-12Y, G. G-20, H. Jumbo cultivars. I and J are adaxial and abaxial leaf surfaces of G-20 cultivar at a higher magnification (3000 X). Black arrows indicate stomata; white arrows indicate polyhedral inclusions. (A-H: 1100 X; I-J: 3000X).

The cuticle, which is made up of cutin, a polyester that is partly covered and interspersed with waxes, epicuticular and intracuticular waxes, varies among plant species. Secondary metabolites, such as flavonoids and triterpenoids, have been found among the wax components in different plant species (Samuels *et al.*, 2008). The presence of Silicon (Si) layer along with cuticles has been found effective in preventing fungal pathogen invasion (Wang *et al.*, 2017). The removal of epicuticular wax resulted in increasing the level of aflatoxin in corn kernel, indicating the importance of epicuticular wax to prevent fungal contamination (Gomes *et al.*, 2012). However, different studies have shown that the cutin monomers induce the germination of various pathogenic fungus such as *Magnaporthe grisea* and *Colletotrichum trifolii* (Gilbert *et al.*, 1996; Dickman *et al.*, 2003). Besides cutin monomers, surface waxes were also found to activate the development of *C. gloeosporioides*, a pathogen of avocado (Podila *et al.*, 1993). The difference in the types of cuticle layer between adaxial and

abaxial surfaces could provide information regarding their roles. The adaxial surface is directly in contact with stress such as UV radiation, insect and pest penetration, etc. Thus, the presence of additional wax crystalloids in the upper surface could help leaves add an additional layer of defense against biotic and abiotic stress.

3.2. Inclusions

The leaf samples, when magnified at 400X, revealed the presence of inclusions on the adaxial and abaxial leaf surface (Fig. 3 and 4). The inclusions exhibited distinct patterns for each cultivar, which further proceeded for their elemental analysis. The inclusion present on the leaf margin of the Jumbo peanut cultivar was observed to be higher compared to Georgia cultivars (Fig. 3 A-D). Whereas, in lamina higher density of inclusions were observed in Georgia cultivars compared to the Jumbo cultivar (Fig. 3). SEM/EDX investigation provided the weight concentration (%) for calcium and silicon present in the inclusions (Table 3). The elemental analysis revealed the highest weight concentration of calcium in the inclusions of Jumbo cultivar on the margin (12.28±3.33) while the lowest was observed in the inclusions of the midrib of G-06 cultivar (2.87±0.34). Similarly, the highest weight concentration of silicon was found in the inclusions of Jumbo cultivar on the margin (13.61±2.28) while the lowest was observed in the inclusions of the margin of G-12Y cultivar (0.14±0.04). The study found significant differences in the weight concentration of calcium among different cultivars of peanuts whereas no significant differences were found for silicon.

It has also been reported that the leaves of both *Amaranthus* spp. and *Vitis vinifera* exhibited a comparable pattern of inclusions. The inclusions are made up of carbon-calcium compounds, specifically calcium oxalate crystals or cystoliths that contain calcium carbonate. Upon closer analysis of these inclusions, it was observed that there was a notable augmentation in photosynthesis in correlation with the overall area of the inclusions. Inclusions help to provide a layer of defense against infections and insects. The patterns of inclusion in the leaves exhibit similarities as density increases and leaf maturation occurs (Giannopoulos *et al.*, 2019). We wanted to confirm the presence of inclusions and their chemical nature that were observed through clearing. Samples were processed for SEM without fixation and dehydration to ascertain the presence of inclusions, their elemental analysis, and study of the cuticle which might have caused the wrinkles (Fig. 3, 4, and 7). Calcium and silicon have been shown to play a crucial role in inhibiting the growth

Table 3: Weight concentration (%) of Calcium (Ca) and Silicon (Si) inclusions on abaxial leaf surface. The data is presented as Mean ± S.E.

Cultivars	*G-06*			*G-12Y*			*G-20*			*Jumbo*		
Part of the leaf	Margin	Lamina	Midrib	Margin	Lamina	Midrib	Margin	Lamina	Midrib	Margin	Lamina	Midrib
Calcium	7.53±0.89	6.30±0.52	2.87±0.34	7.26±2.63	3.21±3.21	7.11±0.56	6.94±1.13	Absent	5.05±0.987	12.28±3.33	7.413±0.58	8.14±2.09
Silicon	0.35±0.10	0.27±0.03	0.40±0.31	0.14±0.04	0.35±0.25	0.21±0.04	0.44±0.24	0.91±0.76	Absent	13.61±2.28	0.661±0.33	0.32±0.08

of pathogens (Chain *et al.*, 2009; Jiang *et al.*, 2013). In the current study, the presence of calcium and silicon in the inclusions with variations among the cultivars was observed, which may deter chewing insects responsible for the spread of the fungus inadvertently. As larvae feed on infected leaves, fungal spores and mycelia can adhere to their bodies, legs, and mouthparts. When these larvae move to other leaves or plants, they can passively transfer the attached spores to new locations, potentially initiating new infections. This could suggest their roles and differences in the level of defense against biotic stress.

3.3. Image Analysis

This study evaluated the performance of two separate convolutional neural network (CNN) structures in accurately categorizing stomata images into four distinct groups. The initial architecture, known as Model 1, integrated batch normalization and adapted dropout techniques. The second architecture, referred to as Model 2, employed the RMSprop optimization algorithm with a modified learning rate. The efficacy of these models was assessed using precision, recall, and F1 score essential metrics for measuring the accuracy of classification models (Table 4). Model 1 demonstrated outstanding performance in the G-06 stomata category, achieving perfect scores of 100% in precision, recall, and F1 score. It exhibited flawless identification with no misclassifications. Nevertheless, when tested on G-12Y stomata, the system exhibited impeccable precision but a reduced recall rate of 73%, suggesting that it failed to discover numerous genuine cases. The difference led to a decrease in the F1 score to 84%. The precision of G-20 stomata reduced somewhat to 95%, while the recall declined more considerably to 61%, resulting in a F1 score of 74%. The performance on Jumbo stomata was characterized by a precision rate of 60%, indicating a significant number of false positives. However, it was compensated by a high recall rate of 97%, resulting in a F1 score of 74%.

Model 2, on the other hand, demonstrated excellent performance, achieving F1 values of 98 and 97 for G-06 and G-12Y stomata, respectively. This indicates a well-balanced performance, although there was a minor decrease in precision for G-06 compared to Model 1. Model 2 demonstrated exceptional performance by achieving a flawless recall rate of 100% for G-12Y stomata, outperforming Model 1 and displaying superior detection abilities for this specific category. However, the performance of the system on G-20 and Jumbo stomata was not as good, as indicated by F1 values of 79 and 74, respectively. These ratings indicate a performance that is both balanced and poor in terms of precision

and recall for these areas. Model 1's utilization of batch normalization and modified dropout was highly effective in achieving specificity, particularly for G-06 and G-12Y stomata. This ensured precise categorization when the model identified an image as belonging to these specific categories. Nevertheless, its sensitivity was diminished, particularly for G-12Y stomata, as it was unable to identify a substantial proportion of accurate occurrences. This problem was especially severe for G-20 stomata, as both the sensitivity (recall) and the resulting F1 score were negatively impacted. Despite the difficulties encountered, Model 1 had a remarkable capacity to accurately identify nearly all genuine occurrences of Jumbo stomata (high recall), however it incorrectly identified a significant proportion of non-Jumbo photos (poor accuracy). In contrast, the approach employed by Model 2, utilizing RMSprop with a modified learning rate, yielded a more equitable balance between sensitivity and specificity. The method demonstrated exceptional efficacy in identifying G-12Y stomata, obtaining flawless recall. This indicates an improved ability to generalize and accurately classify all occurrences belonging to this category. Nevertheless, the well-rounded performance of Model 2 also brought attention to challenges in precisely distinguishing G-20 and Jumbo stomata. Both precision and recall were moderate, suggesting room for improvement. This study's findings emphasize the inherent trade-offs that exist between sensitivity and specificity in classification tasks. The selection between the two Models would ultimately hinge on individual research requirements—whether the priority is to minimize incorrect positive results or incorrect negative results. Furthermore, the diverse performance observed among different stomata categories highlights the necessity for ongoing optimization of the Models. This could involve investigating combination or hybrid approaches that utilize the advantages of both batch normalization, dropout, and RMSprop optimization strategies.

Table 4: Comparative summary of performance matrix for the developed CNN classification models developed for stomata

Peanut cultivars	*Batch normalization with adjusted dropout method*			*RMSprop with adjusted learning rate*		
	Precision	*Recall*	*F1 score*	*Precision*	*Recall*	*F1 score*
G-06 stomata	100	100	100	95	100	98
G-12Y stomata	100	73	84	94	100	97
G-20 stomata	95	61	74	81	78	79
Jumbo stomata	60	97	74	78	71	74

The fundamental component of a CNN is the convolutional layer, which utilizes a sequence of learnable filters (kernels) that convolve over the input image. These filters do localized computations to identify features such as edges, textures, and basic forms. As layers accumulate, the network progressively constructs more abstract and intricate representations, transitioning from fundamental visual signals in the first levels to advanced information such as object components in deeper layers. This hierarchical learning methodology allows CNNs to generalize effectively across varied visual situations and has been thoroughly illustrated and corroborated in seminal research (Zeiler *et al.*, 2014). After each convolution operation, activation functions like the (ReLU) incorporate non-linearity, enabling the network to represent intricate and nonlinear patterns within the data. Rectified Linear Unit has become the standard in CNNs owing to its computational efficiency and capacity to alleviate vanishing gradient problems, in contrast to traditional activation functions such as sigmoid and tanh (Nair and Hinton, 2010). To manage the computational complexity and enhance the model's robustness, CNNs incorporate pooling layers that reduce the spatial resolution of the feature maps. The predominant technique, max pooling, preserves the most significant characteristic within a specific area, thereby reducing the number of parameters and facilitating spatial invariance. This characteristic allows the network to identify features irrespective of their location within the input image (Scherer *et al.*, 2010). Training CNNs entails improving the weights of filters and neurons through gradient descent and backpropagation algorithms, utilizing loss functions such as category cross-entropy to direct the learning process (Rumelhart *et al.*, 1986; LeCun *et al.*, 2015). To mitigate overfitting and enhance generalization, regularization methods like dropout are utilized, which randomly deactivate some neurons during training, prompting the network to acquire redundant and resilient features (Hinton *et al.*, 2012). Consequently, these architectural innovations have enabled CNNs to perform exceptionally in several benchmark datasets and practical applications.

Aside from their dominance in traditional computer vision tasks, CNNs have been effectively adapted for a variety of fields. In biomedical imaging, they are used for disease detection, histopathology slide analysis, and organ segmentation (Litjens *et al.*, 2017). In remote sensing, CNNs enhance land cover classification and object detection in satellite imagery (Zhang *et al.*, 2016). The agricultural industry has seen significant benefits, with CNNs used for plant disease detection, weed classification, and crop production estimation (Kamilaris and Prenafeta-Boldú, 2018). These diverse applications underscore the versatility and scalability of CNNs, which remain a fundamental tool in artificial intelligence research and development across several fields.

The utilization of deep learning (DL) in plant image analysis has progressed rapidly, with recent works developing tools to automate trichome and stomatal phenotyping. Xu *et al.*, 2023 presented TrichomeYOLO, an object detection network based on YOLOv5, augmented with Transformer modules and a bidirectional feature pyramid network (BiFPN) for the identification of maize trichomes in scanning electron microscopy (SEM) images. Although their model attained an accuracy of 92.1%, surpassing several prominent object identification models, the performance assessment was restricted to overall detection rates, lacking comprehensive diagnostics on the model's sensitivity to trichome morphological variation or the trade-offs between false positives and false negatives. Garcia *et al.*, 2022 devised a semi-automated method for quantifying trichomes in *Arabidopsis thaliana* with a tandem Ilastik-Fiji approach. Although the technique was intuitive and accessible for fundamental picture segmentation, it predominantly depended on manual annotation and lacked a deep learning framework, class-specific accuracy evaluation, or scalability for many phenotypes.

Malagol *et al.*, 2025 utilized a ResNet-based convolutional neural network in a high-throughput method to estimate abaxial leaf hair coverage in grapevine leaf discs, demonstrating a robust correlation with expert assessments (R = 0.98 and 0.92 for two evaluators) and a root-mean-square error below 15%. Nonetheless, their model performance was encapsulated by accuracy and error metrics, lacking differentiation among leaf types, hair density classifications, or trends in model misclassification—data essential for diagnostic application or cultivar-specific phenotyping. Using microscopic pictures, Gibbs *et al.*, 2021 introduced a semantic segmentation pipeline to assess maximal stomatal conductance (gsmax) in wheat and poplar leaves. Their model attained near-equivalence with expert measures, deviating by under 4%. Nevertheless, the investigation concentrated on functional outputs (gsmax) and did not disclose class-specific performance or evaluate architectural alternatives.

Gibbs and Burgess, 2024 combine the current status of deep learning in stomatal research in their extensive review. They classify architectures such as YOLO, UNet, and VGG by application, such as object detection, semantic segmentation, or instance segmentation, and highlight the necessity for open datasets and standardization. This review highlighted the technical diversity of pipelines while emphasizing a significant deficiency in the field: inadequate interpretability of performance outputs, insufficient use of class-wise evaluation measures, and minimal discourse on the trade-offs associated with model design choices.

The present research directly focuses on these shortcomings by offering a comprehensive comparative assessment of two alternative CNN architectures: Model 1, which integrates batch normalization and adjusted dropout, and Model 2, which employs the RMSprop optimizer with an adjusted learning rate, across various stomatal phenotypes. Instead of depending exclusively on overall accuracy or visual overlays, we present class-specific precision, recall, and F1-score metrics, which elucidate significant disparities in the models' management of morphological variability. For instance, although Model 1 attained flawless classification (100% precision, recall, F1) for G-06 stomata, its recall for G-12Y decreased to 73%, showing a propensity to overlook instances of this class. This finding is significant as it indicates that Model 1 may not be the best choice for tasks where identifying G-12Y stomata is crucial. Conversely, Model 2 attained 100% recall and a superior F1-score (97%) for G-12Y, although a marginal rise in false positives. In the more demanding G-20 class, Model 2 exhibited enhanced recall (78% compared to 61% for Model 1), underscoring its resilience in handling confusing shapes. This finding is significant as it suggests that Model 2 may be more suitable for tasks where identifying G-20 stomata is important. These subtle findings are both physiologically significant and illustrate the constraints of model generalization across stomatal types, which is beneficial for breeding programs, where the relative costs of missing vs wrong identifications may differ by feature. Moreover, our study directly connects the model's behavior and the design features: Model 1 uses regularization to provide enhanced precision, which is advantageous when false positives are expensive, but Model 2's adaptive learning approach enhances memory, which is beneficial for comprehensive screening tasks. These distinctions enable end users to select models tailored to their particular study or breeding setting and highlight our research's adaptability. Our pipeline exhibits both automation and interpretability, deployability and adaptability, distinguishing it from previous work and embodying the characteristics of next-generation phenotyping tools. Although the CNN models were trained and validated using in-house microscope images, acquiring high-resolution stomatal images directly from field-grown plants remains technically challenging. Nevertheless, these models establish a baseline for future automated phenotyping efforts and can be expanded as more diverse datasets become available.

4. Conclusion

Micromorphological study on four peanut cultivars, using light, and Scanning Electron Microscopy analyses, provides valuable insights into the differences

in plant surface topography that can play a role in the potential defense mechanisms against disease causing microbes such as *A. flavus*, *A. parasiticus*, *A. niger*. Micromorphological studies revealed the presence of non-glandular trichomes on leaves of all the cultivars studied, but with variations in size and density. Scanning electron microscopy further characterized the surface morphology of the leaf samples, revealing the presence of specific inclusions with distinct patterns across cultivars. SEM/EDX study revealed the elemental composition of these inclusions, which contained significant amounts of calcium and silicon, both of which are involved in pathogen restriction and signaling pathways. SEM analysis of the presence of cuticle and cuticular wax micromorphology in leaves of peanut cultivars revealed heterogeneity among cultivars. These differences could be attributed to their composition, which could play various roles in preventing microbial invasion or infection. This study could help identify tolerant and susceptible peanut cultivars to fungal infection, as well as providing insight into the many approaches that could be employed in these studies. Stomatal studies confirmed the distribution and type of stomata on both leaf surfaces (adaxial and abaxial) with a predominant occurrence of paracytic stomata. In general, all the cultivars studied showed a higher number of stomata on the abaxial leaf surface. Among all four cultivars, stomatal density across cultivars revealed significant differences, G-06 scoring the highest. The abaxial surface had more stomata than the adaxial surface except G-20, suggesting cultivar-specific features may affect stomatal distribution.

***Author Contributions**:* TA: Graduate student, carried out plant growing, collection of materials and optimized clearing protocols, generation of data and writing first draft; BS: Graduate student, optimized electron microscopic protocols and data generation, co-wrote the first draft; PK: Training graduate students, data validation, and manuscript review; AS: CNN model development, guiding TA, and manuscript review; TT: Providing facilities for CNN research and manuscript review; NJ: Conceptualizing the project, data finalization, manuscript review, and providing lab facilities and resources.

***Funding**:* Reducing Aflatoxin Contamination in United States Peanuts, USDA (United States Department of Agriculture) REE, Accession No. 440638. The funders had no role in study design, data collection and analysis, decision to publish, or preparation of the manuscript.

***Data Availability Statement**:* The raw data supporting the conclusions of this article will be made available by the authors on request.

Acknowledgments

We thank Ms. Ashvini Pawar for help with electron microscopy at the Center for Ultrastructural Research (CURE), Fort Valley State University.

Conflicts of Interest: The authors declare that they have no competing interests.

References

Akram NA, Shafiq F and Ashraf M. 2018. Peanut (Arachis hypogaea L.): A prospective legume crop to offer multiple health benefits under changing climate. Comprehensive Reviews in Food Science and Food Safety, 17, 1325-1338.

Andayani U, Sumantri IB, Pahala A and Muchtar MA. 2020. The implementation of deep learning using convolutional neural network to classify based on stomata microscopic image of curcuma herbal plants. IOP Conference Series: Materials Science and Engineering, 851, 012035.

Arya GC, Sarkar S, Manasherova E, Aharoni A and Cohen H. 2021. The plant cuticle: An ancient guardian barrier set against long standing rivals. Frontiers in Plant Science, 12, 663165.

Ayoola PB, Adeyeye A and Onawumi OO. 2012. Chemical evaluation of food value of groundnut (*Arachis hypogaea* L.) seeds. American Journal of Food and Nutrition, 2, 55-57.

Banerji ML and Das S. 1972. Minor venation pattern in the Indian Acers. Advances in Plant Morphology, 51-57.

Bickford CP. 2016. Ecophysiology of leaf trichomes. Functional Plant Biology, 43, 807–814.

Chain F, Côté-Beaulieu C, Belzile F, Menzies JG and Bélanger RR. 2009. A comprehensive transcriptomic analysis of the effect of silicon on wheat plants under control and pathogen stress conditions. Molecular Plant-Microbe Interactions, 22, 1323–1330.

Chen G, Chen P, Shi Y, Hsieh CY, Liao B and Zhang S. 2019. Rethinking the usage of batch normalization and dropout in the training of deep neural networks. arXiv preprint arXiv:1905.05928.

Davis JP, Price KM, Dean LL, Sweigart DS, Cottonaro JM and Sanders TH. 2016. Peanut oil stability and physical properties across a range of industrially relevant oleic acid/linoleic acid ratios. Peanut Science, 43, 1–11.

Dehgahi R, Subramaniam S, Zakaria L, Joniyas A, Firouzjahi FB, Haghnama K and Razinataj M. 2015. Review of research on fungal pathogen attack and plant defense mechanism against pathogen. International Journal of Science Research in Agricultural Sciences, 2, 197–208.

Dickman MB, Ha YS, Yang Z, Adams B and Huang C. 2003. A protein kinase from *Colletotrichum trifolii* is induced by plant cutin and is required for appressorium formation. Molecular Plant-Microbe Interactions, 16, 411–421.

Driesen E, Van den Ende W, De Proft M and Saeys W. 2020. Influence of environmental factors light, CO_2, temperature, and relative humidity on stomatal opening and development: A review. Agronomy, 10, 1975.

Esau K. 1977. Anatomy of Seed Plants. 2nd ed. John Wiley and Sons, New York (USA), 445–448.

Foreign Agricultural Service USDA. 2023. Peanut World Production 2023. Available online:https://ipad.fas.usda.gov/cropexplorer/cropview/commodityView.aspx?cropid=2221000&sel_year=2023&rankby=Production (accessed on 7 July 2025).

Franks PJ and Farquhar GD. 2007. The mechanical diversity of stomata and its significance in gas-exchange control. Plant Physiology, 143, 78–87.

Gabler FM, Smilanick JL, Mansour M, Ramming DW and Mackey BE. 2003. Correlations of morphological, anatomical, and chemical features of grape berries with resistance to *Botrytis cinerea*. Phytopathology, 93, 1263–1273.

Garcia A, Talavera-Mateo L and Santamaria ME. 2022. An automatic method to quantify trichomes in *Arabidopsis thaliana*. Plant Science, 323, 111391.

Giannopoulos A, Bresta P, Nikolopoulos D, Liakopoulos G, Fasseas C and Karabourniotis G. 2019. Changes in the properties of calcium-carbon inclusions during leaf development and their possible relationship with leaf functional maturation in three inclusion-bearing species. Protoplasma, 256, 349–358.

Gibbs JA and Burgess AJ. 2024. Application of deep learning for the analysis of stomata: A review of current methods and future directions. Journal of Experimental Botany, 75, 6704–6718.

Gibbs JA, McAusland L, Robles-Zazueta CA, Murchie EH and Burgess AJ. 2021. A deep learning method for fully automatic stomatal morphometry and maximal conductance estimation. Frontiers in Plant Science, 12, 780180.

Gilbert RD, Johnson AM and Dean RA. 1996. Chemical signals responsible for appressorium formation in the rice blast fungus *Magnaporthe grisea*. Physiological and Molecular Plant Pathology, 48, 335–346.

Goh YK. 2001. The role of kernel epicuticular wax in *Zea mays* resistance to *Aspergillus flavus* and aflatoxin production. Louisiana State University, Baton Rouge, USA.

Gomes S, Bacelar E, Martins-Lopes P, Carvalho T and Guedes-Pinto H. 2012. Infection process of olive fruits by *Colletotrichum acutatum* and the protective role of the cuticle and epidermis. Journal of Agricultural Science, 4, 101.

Goodfellow I, Bengio Y and Courville A. 2016. Deep Learning. Cambridge (MA): MIT Press.

Gray A, Liu L and Facette M. 2020. Flanking support: how subsidiary cells contribute to stomatal form and function. Frontiers in Plant Science, 11, 881.

Hinton GE, Srivastava N, Krizhevsky A, Sutskever I and Salakhutdinov RR. 2012. Improving neural networks by preventing co-adaptation of feature detectors. arXiv preprint arXiv:1207.0580.

Isanga J and Zhang GN. 2007. Biologically active components and nutraceuticals in peanuts and related products. Food Reviews International, 23, 123–140.

Jiang JF, Li JG and Dong YH. 2013. Effect of calcium nutrition on resistance of tomato against bacterial wilt induced by *Ralstonia solanacearum*. European Journal of Plant Pathology, 136, 547–555.

Jiang X, Chang L and Zhang YD. 2020. Classification of Alzheimer's disease via eight-layer convolutional neural network with batch normalization and dropout techniques. Journal of Medical Imaging and Health Informatics, 10(5), 1040–1048.

Kamilaris A and Prenafeta-Boldú FX. 2018. Deep learning in agriculture: A survey. Computers and Electronics in Agriculture, 147, 70–90.

Karabourniotis G, Bornman JF and Liakoura V. 1999. Different leaf surface characteristics of three grape cultivars affect leaf optical properties as measured with fibre optics: Possible implication in stress tolerance. Australian Journal of Plant Physiology, 26, 47–53.

Kim KW. 2019. Plant trichomes as microbial habitats and infection sites. European Journal of Plant Pathology, 154, 157–169.

Kortekamp A and Zyprian E. 1999. Leaf hairs as a basic protective barrier against downy mildew of grapes. Journal of Phytopathology, 147, 453–459.

LeCun Y, Bengio Y and Hinton G. 2015. Deep learning. Nature, 521, 436–444.

LeCun Y, Bottou L, Bengio Y and Haffner P. 1998. Gradient-based learning applied to document recognition. Proceedings of the IEEE, 86, 2278–2324.

Liakopoulos G, Stavrianakou S and Karabourniotis G. 2006. Trichome layers versus dehaired lamina of *Olea europaea* leaves: Differences in flavonoid distribution, UV-absorbing capacity, and wax yield. Environmental and Experimental Botany, 55, 294–304.

Liang X, Zhou G and Pan R. 2003. Wax and cuticle of peanut seed coat in relation to infection and aflatoxin production by *Aspergillus flavus*. Journal of Tropical and Subtropical Botany, 11, 11–14.

Litjens G, Kooi T, Bejnordi BE, Setio AAA, Ciompi F and Ghafoorian M, Sánchez CI. 2017. A survey on deep learning in medical image analysis. Medical Image Analysis, 42, 60–88.

Liu Y, Liu K and Zhao Y. 2022. Effect of storage conditions on the protein composition and structure of peanuts. ACS Omega, 7, 21694–21700.

Malagol N, Rao T, Werner A, Töpfer R and Hausmann L. 2025. A high-throughput ResNet CNN approach for automated grapevine leaf hair quantification. Scientific Reports, 15, 1590.

Meddya S, Meshram S, Sarkar D, Datta R, Singh S, Avinash G, Kumar Kondeti A, Savani AK and Thulasinathan T. 2023. Plant stomata: An unrealized possibility in plant defense against invading pathogens and stress tolerance. Plants, 12, 3380.

Melotto M, Underwood W, Koczan J, Nomura K and He SY. 2006. Plant stomata functions in innate immunity against bacterial invasion. Cell, 126, 969–980.

Nair V and Hinton GE. 2010. Rectified linear units improve restricted Boltzmann machines. In: Proceedings of the 27th International Conference on Machine Learning (ICML-10). Madison (WI): Omnipress, Haifa, Israel, 807–814.

Patel I, Gorim LY, Tanino K and Vandenberg A. 2021. Diversity in surface microstructures of trichomes, epidermal cells, and stomata in lentil germplasm. Frontiers in Plant Science, 1, 697692.

Paul V, Sharma L, Pandey R and Meena RC. 2017. Measurements of stomatal density and stomatal index on leaf/plant surfaces. In: Manual of ICAR Sponsored Training Programme for Technical Staff of ICAR Institutes on Physiological Techniques to Analyze the Impact of Climate Change on Crop Plants, 27.

Podila GK, Rogers LM and Kolattukudy PE. 1993. Chemical signals from avocado surface wax trigger germination and appressorium formation in *Colletotrichum gloeosporioides*. Plant Physiology, 103, 267–272.

Raghu M, Unterthiner T, Kornblith S, Zhang C and Dosovitskiy A. 2021. Do vision transformers see like convolutional neural networks? Advances in Neural Information Processing Systems, 34, 12116–12128.

Rao VR and Murty UR. 1994. Botany, morphology and anatomy. In: Smartt J, editor. The Groundnut Crop. Springer, Dordrecht (Netherlands), 43–95.

Rumelhart DE, Hinton GE and Williams RJ. 1986. Learning representations by back-propagating errors. Nature, 323, 533–536.

Sack FD. 1987. The development and structure of stomata. In: Zeiger E, Farquhar GD and Cowan IR, editors. Stomatal Function. Stanford University Press, Stanford (USA), 59–89.

Salisbury EJ. 1928. On the causes and ecological significance of stomatal frequency, with special reference to the woodland flora. Transactions of the Royal Society of London B, 216, 1–65.

Samuels L, Kunst L and Jetter R. 2008. Sealing plant surfaces: Cuticular wax formation by epidermal cells. Annual Review of Plant Biology, 59, 683–707.

Scherer D, Müller A and Behnke S. 2010. Evaluation of pooling operations in convolutional architectures for object recognition. In: Proceedings of the International Conference on Artificial Neural Networks, Berlin, Germany, September 2010. Berlin (Germany): Springer, 92–101.

Sehgal L and Paliwal GS. 1974. Studies on the leaf anatomy of *Euphorbia*: II. Venation patterns. Botanical Journal of the Linnean Society, 68, 173–208.

Siddique A, Cook K, Holt Y, Panda SS, Mahapatra AK, Morgan ER, van Wyk JA and Terrill TH. 2024. From plants to pixels: the role of artificial intelligence in identifying *Sericea Lespedeza* in field-based studies. Agronomy, 14(5), 992.

Singh V, Jain DK and Sharma M. 1976. Leaf architecture in *Salix*. Journal of the Indian Botanical Society, 55, 140–150.

Subrahmanyam P, Smith DH, Raber RA and Shepherd E. 1987. An outbreak of yellow mold of peanut seedlings in Texas. Mycopathologia, 100(2), 97–102.

Underwood W, Melotto M and He SY. 2007. Role of plant stomata in bacterial invasion. Cellular Microbiology, 9, 1621–1629.

Vaidya BN, Jackson CL, Perry ZD, Dhekney SA and Joshee N. 2016. Agrobacterium-mediated transformation of thin cell layer explants of *Scutellaria ocmulgee* small: A rare plant with anti-tumor properties. Plant Cell, Tissue and Organ Culture, 127, 57–69.

Vasco A, Thadeo M, Conover M and Daly DC. 2014. Preparation of samples for leaf architecture studies, a method for mounting cleared leaves. Applications in Plant Sciences, 2, 1400038.

Voronkov AS, Kumachova TK and Ivanova TV. 2020. Plant passive immunity: Micromorphological and biochemical features of the Maloideae (Rosaceae) external tissues. Current Research Trends in Biological Sciences, 1–16.

Wang M, Gao L, Dong S, Sun Y, Shen Q and Guo S. 2017. Role of silicon on plant–pathogen interactions. Frontiers in Plant Science, 8, 701.

Wang X, Shen C, Meng P, Tan G and Lv L. 2021. Analysis and review of trichomes in plants. BMC Plant Biology, 21(1), 70.

Xu J, Yao J, Zhai H, Li Q, Xu Q, Xiang Y and Lu Y. 2023. TrichomeYOLO: A neural network for automatic maize trichome counting. Plant Phenomics, 5, 0024.

Zeiler MD and Fergus R. 2014. Visualizing and understanding convolutional networks. In: Fleet D, Pajdla T, Schiele B and Tuytelaars T, editors. Computer Vision–ECCV 2014: 13th European Conference, Zurich, Switzerland, September 2014, Proceedings, Part I. Springer International Publishing, Cham (Switzerland), 818–833.

Zhang L, Zhang L and Du B. 2016. Deep learning for remote sensing data: A technical tutorial on the state of the art. IEEE Geoscience and Remote Sensing Magazine, 4, 22–40.